

**ARTIFICIAL ANALOGUES OF THE OXYGEN-EVOLVING COMPLEX
IN PHOTOSYNTHESIS: THE OXO-BRIDGED RUTHENIUM DIMER
 $L_2(H_2O)Ru^{III}-O-Ru^{III}(H_2O)L_2$, $L = 2,2'$ -BIPYRIDYL-4,4'-
DICARBOXYLATE**

PASCAL COMTE, MOHAMMAD K. NAZEERUDDIN, FRANCOIS P. ROTZINGER,
ARTHUR J. FRANK* and MICHAEL GRÄTZEL**

*Institut de Chimie Physique, Ecole Polytechnique Fédérale, CH-1015 Lausanne
(Switzerland)*

Summary

Controlled potential electrolysis of acidic solutions of *cis*-diaquabis-(2,2'-bipyridyl-4,4'-dicarboxylate) yields the title compound **1** in quantitative yield. The dimer was isolated as the sulfate salt and characterized. It is distinguished by a high activity, even under neutral and alkaline conditions where the turnover numbers achieved are the highest reported so far for homogeneous water oxidation catalysts. Because this property is paired with an excellent catalytic activity for the oxidation of water to oxygen, **1** constitutes an intriguing example of a molecular species matching the performance of the oxygen-evolving complex of photosystem II in natural photosynthesis.

Introduction

In the field of artificial photosynthesis, attempts are currently being made to design molecular units that mimic the function of the oxygen-evolving complex (OEC), a key constituent of the plant photosystem II. It is generally agreed that the OEC is constituted by at least two manganese ions acting as the storage centers for the four redox equivalents required to bring about the release of oxygen from two water molecules [1]. The OEC has been shown to operate by stepwise accumulation of positive charges and release of protons [2]. Structural features of the OEC complex are now under intensive investigation [3, 4].

Although several intriguing molecular models bearing similarity to the OEC have been synthesized [5 - 7], these manganese complexes do not

*Visiting professor, on leave of absence from the Solar Energy Research Institute, Golden CO, U.S.A.

**Author to whom correspondence should be addressed.

display the catalytic properties of their natural counterpart. On the other hand, a number of ruthenium compounds have been identified that promote the oxidation of water to oxygen [8]. Among the complexes being investigated, oxo-bridged dimers with bipyridyl ligands are receiving increasing attention [9, 10] since the discovery of this class of compounds [11]. The presence of two Ru centers with aqua ligands and multiple redox states makes these complexes attractive candidates for water-oxidation catalysis. We report here on a new oxo-bridged Ru dimer with outstanding stability and activity approaching the turnover frequency of the oxygen-evolving complex in natural photosynthesis.

Experimental section

Materials

Cis-diaquabis(2,2'-bipyridyl-4,4'-dicarboxylate) ruthenium(II), *cis*-Ru^{II}-L₂(H₂O)₂, was synthesized as previously described [12]. The dimer L₂(H₂O)-Ru^{III}-O-Ru^{III}(H₂O)L₂ was obtained by oxidative electrolysis of 2×10^{-3} M *cis*-Ru^{II}L₂(H₂O)₂ in 0.5 M H₂SO₄. 50 ml of solution was introduced into a double-walled Pyrex cell connected to a thermostat adjusted to 40 °C. The solution was protected from light to avoid *cis-trans* isomerization during the electrolysis. The cell was purged continuously with Ar to prevent accumulation of hydrogen formed at the counterelectrode. A saturated Na₂SO₄/HgSO₄/Hg reference electrode was employed. The working electrode, a Pt gauze, was kept at 1.1 V (SCE) and the electrolysis was stopped after 15 h when conversion to the dimer was complete. The product of the electrolysis is a sulfate complex of the mixed valency μ -oxo dimer with oxidation states III and IV for the Ru. Reduction at 0.6 V gives L₂(H₂O)-Ru^{III}-O-Ru^{III}(H₂O)L₂. Isolation of the dimer was achieved by concentrating the solution to a volume of 15 ml in a Rotavap (bath temperature 40 °C) and cooling overnight in the refrigerator. Spontaneous precipitation of bluish-green microcrystals of [L₂(H₂O)Ru^{III}-O-Ru^{III}(H₂O)L₂]⁴⁺(SO₄²⁻)₂ occurred. The microcrystals were collected by filtration through a G4 sintered glass frit and washed thoroughly first with 120 ml portions of 4:1 and 1:1 acetone/diethyl ether mixtures and finally with dry diethyl ether. Subsequent drying under vacuum yielded 67 mg of product. To the filtrate, 1 g of Na₂SO₄ was added and left in the refrigerator for 50 h. The precipitate was collected as described, yielding an additional 25 mg of product. The total yield of isolated dimer is 70% of the theoretical value. Elemental analysis for C₄₈H₃₆N₈O₂₇S₂Ru₂·9H₂O yielded: C, 36.4; H, 3.4; N, 7.2; S, 4.2%; calculated: C, 36.37; H, 3.43; N, 7.07; S, 4.05%. The carbon to nitrogen ratio of 5.95 (calculated value 6) indicates that no decarboxylation took place during the preparation of the dimer. All other materials were reagent grade and used without further purification.

Apparatus

Ultraviolet-visible absorption spectra were measured with a HP 8450 A diode-array spectrophotometer. The infrared spectra were recorded on a

Perkin-Elmer 684 instrument and the sample was prepared in KBr pellets. Electrochemical experiments employed a Wenking POS-73 potentiostat and a three-electrode, two-compartment cell. The working electrode for cyclic voltammetry was In-doped SnO_2 (0.7 cm^2 surface area, Balzers AG, FL). A saturated $\text{Na}_2\text{SO}_4/\text{HgSO}_4/\text{Hg}$ reference electrode was employed throughout to avoid chlorine contamination. The solutions were deaerated by Ar bubbling. All electrode potentials reported below are referenced to SCE.

Illuminations were performed with a 150-W tungsten halogen lamp equipped with a water jacket and a 450-nm cutoff filter to remove IR and UV radiation, respectively. The solution (10 ml) was contained in a 20 ml Pyrex vessel and was freed from oxygen by bubbling with Ar prior to photolysis. Temperature was maintained at 25°C by means of a thermostat.

Oxygen production was monitored with a Clark-type sensor (Yellow Springs Instruments, YSI Model 83) placed in the head space above the solution. The results were corroborated by GC measurements. The GC was equipped with a thermal conductivity detector and Ar carrier gas. Air leakage was negligible during the time of the experiment and made no significant contribution to the observed oxygen-evolution rates.

Results and discussion

Absorption and redox properties of $\text{cis-Ru}^{\text{II}}\text{L}_2(\text{H}_2\text{O})_2$

Figure 1 shows the absorption spectrum of $\text{cis-Ru}^{\text{II}}\text{L}_2(\text{H}_2\text{O})_2$ in 1 M $\text{CF}_3\text{SO}_3\text{H}$. Absorption maxima and extinction coefficients are listed in Table 1. For comparison, spectral data for isomeric $\text{cis-Ru}^{\text{II}}\text{L}'_2(\text{H}_2\text{O})_2$, where

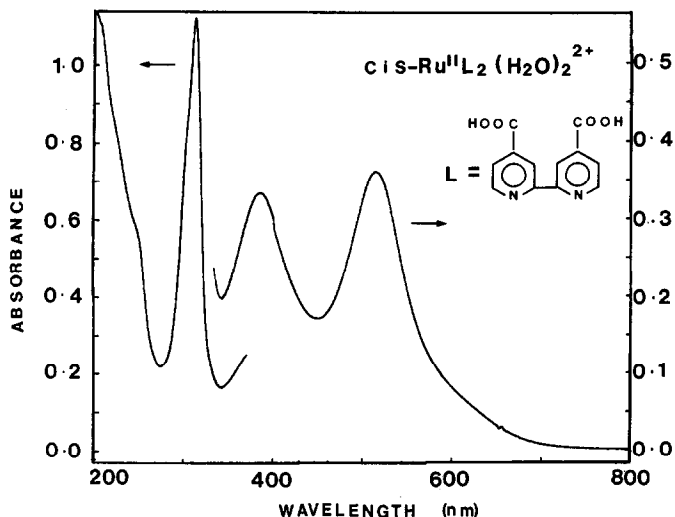


Fig. 1. Absorption spectrum of $3 \times 10^{-5} \text{ M}$ $[\text{cis-Ru}^{\text{II}}\text{L}_2(\text{H}_2\text{O})_2]^{2+}$ in 1 M $\text{CF}_3\text{SO}_3\text{H}$; 1 cm optical pathlength.

TABLE 1

UV-Vis electronic absorption data for $[\text{Ru}^{\text{II}}\text{L}_2(\text{H}_2\text{O})_2]^{\text{a}}$ and related complexes

Complex	Medium	λ_{max} (nm)	ϵ ($\text{M}^{-1} \text{cm}^{-1}$)
$[\text{Ru}^{\text{II}}\text{L}_2(\text{H}_2\text{O})_2]$	1 M $\text{CF}_3\text{SO}_3\text{H}$	514	1.1×10^4
		384	9.8×10^3
		313	3.9×10^4
$[\text{Ru}^{\text{II}}\text{L}'_2(\text{H}_2\text{O})_2]^{\text{b}}$	1 M $\text{CF}_3\text{SO}_3\text{H}$	550	6.0×10^3
		365 (sh)	—
		300	8.0×10^4
$[\text{Ru}^{\text{II}}(\text{bpy})_2(\text{H}_2\text{O})_2]^{\text{c}}$	0.5 M CF_3COOH	480	8.5×10^3
		335	7.7×10^3
		290	5.0×10^4

^aL, L' and bpy = 4,4'-dicarboxy-2,2'-bipyridine, 5,5'-dicarboxy-2,2'-bipyridine and 2,2'-bipyridine, respectively.

^bFrom [10].

^cFrom [13].

L' = 2,2'-bipyridyl-5,5'-dicarboxylic acid and $\text{cis-Ru}^{\text{II}}(\text{bpy})_2(\text{H}_2\text{O})_2$ are also given. In the visible and near UV region, there are two intense bands with maxima at 514 and 384 nm. These distinguish $\text{cis-Ru}^{\text{II}}\text{L}_2(\text{H}_2\text{O})_2$ from the isomeric complex $\text{cis-Ru}^{\text{II}}\text{L}'_2(\text{H}_2\text{O})_2$ which displays only one peak in the wavelength domain above 380 nm. The latter is red-shifted and of weaker intensity than that of $\text{RuL}_2(\text{H}_2\text{O})_2$. The visible absorption can be attributed to the $d(\text{Ru}) \rightarrow \Pi^*$ (bipyridyl-dicarboxylic acid) transition. Similar to $\text{cis-Ru}^{\text{II}}\text{L}'_2(\text{H}_2\text{O})_2$, $\text{cis-Ru}^{\text{II}}\text{L}_2(\text{H}_2\text{O})_2$ shows a very intense and sharp feature in the UV which, however, is located at 313 nm instead of 300 nm. The latter band is ascribed to the ligand $\Pi \rightarrow \Pi^*$ transition. These data illustrate the pronounced effect on the absorption properties exerted by the displacement of the carboxylic acid ligands from the 5,5'- to the 4,4'-position of the bipyridyl ligand. This observation indicates that the location of the COOH substituents influences markedly the electronic energy levels of the complex.

Irradiation of $\text{cis-Ru}^{\text{II}}\text{L}_2(\text{H}_2\text{O})_2$ with $\lambda > 380$ nm light leads to *cis-trans* isomerization. A similar process has been observed for $\text{Ru}^{\text{II}}(\text{bpy})_2(\text{H}_2\text{O})_2$ [13]. In contrast to $\text{cis-Ru}^{\text{II}}\text{L}'_2(\text{H}_2\text{O})_2$, this photoreaction is relatively efficient, and protection of $\text{cis-Ru}^{\text{II}}\text{L}_2(\text{H}_2\text{O})_2$ from light is necessary to avoid conversion to the *trans* isomer. The latter precipitates as a solid upon illumination of aqueous solutions of $\text{cis-Ru}^{\text{II}}\text{L}_2(\text{H}_2\text{O})_2$ at a pH between 4 and 6.5. In this pH domain, the solubility of the *trans* isomer is much less than that of its *cis* analogue.

Figure 2 shows a cyclic voltammogram of $\text{cis-Ru}^{\text{II}}\text{L}_2(\text{H}_2\text{O})_2$ in aqueous 1 M $\text{CF}_3\text{SO}_3\text{H}$. Oxidative and reductive peaks are obtained at 0.87 and 0.77 V, respectively, indicating quasi-reversible behavior. The midpoint potential is at 0.83 V. At pH 4.85, one-electron oxidation occurs at 0.58 V.

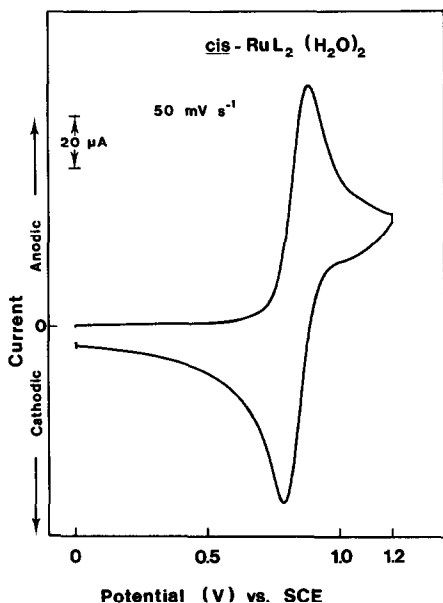
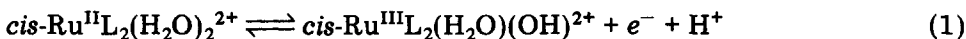


Fig. 2. Cyclic voltammogram of 10^{-3} M $[cis-Ru^{II}L_2(H_2O)_2]^{2+}$ in 1 M CF_3SO_3H In-doped SnO_2 working electrode (1 cm^2 area).

Since the pH value of 1 M CH_3SO_3H is *ca.* 0.3, the shift is 0.058 V/pH, which is close to the value of 59 mV/pH expected for a one-electron oxidation accompanied by the loss of one proton. Presumably, deprotonation occurs at one of the water ligands of the complex, which has a strongly acidic character:



It should be noted that at pH 4.85, $cis-Ru^{II}L_2(H_2O)_2$ is a mono or dianion. Acid-base titration shows that the isoelectric point of the Ru(II) complex is 2.8. Hence, above this pH the molecule is anionic. Combined acid-base titration and spectral analysis indicate that the first water ligand deprotonates above pH 9. This is in agreement with literature data for the unsubstituted $cis-Ru^{II}(bpy)_2(H_2O)_2^{2+}$ and $Ru^{II}(bpy)(py)(H_2O)^{2+}$, for which the first pK values are 11 [14] and 10.3 [15], respectively.

In Table 2, we compare the oxidation of $cis-Ru^{II}L_2(H_2O)_2^{2+}$ with that of the 5,5'-dicarboxylated $cis-Ru^{II}L'_2(H_2O)_2^{2+}$ isomer and the unsubstituted $cis-Ru^{II}(bpy)_2(H_2O)_2^{2+}$ analogue in 1 M acid. The latter exhibits the lowest redox potential followed by $cis-Ru^{II}L'_2(H_2O)_2^{2+}$ and $cis-Ru^{II}L_2(H_2O)_2^{2+}$.

Spectral properties of $cis-Ru^{III}L_2(H_2O)(OH)^{2+}$

The Ru^{III} diaqua complex was produced by controlled potential electrolysis of $cis-Ru^{II}L_2(H_2O)_2^{2+}$ in 1 M CF_3SO_3H at 1 V. A double-walled Pyrex cell was used, which was connected to a thermostat maintained at 25 °C. After 2 h of electrolysis the oxidation was complete, the current being

TABLE 2

Oxidation potentials (V vs. SCE) for $[\text{Ru}^{\text{II}}\text{L}_2(\text{H}_2\text{O})_2]^{\text{a}}$ and related complexes

Compound	Medium	$E_{1/2}$ for $\text{Ru}^{\text{II/III}}$ (V)
$[\text{Ru}^{\text{II}}\text{L}_2(\text{H}_2\text{O})_2]$	1 M HCF_3SO_3	0.83
$[\text{Ru}^{\text{II}}\text{L}'_2(\text{H}_2\text{O})_2]^{\text{b}}$	0.5 M H_2SO_4	0.78
$[\text{Ru}^{\text{II}}(\text{bpy})_2(\text{H}_2\text{O})_2]^{\text{c}}$	1 M HCF_3COO	0.63

^aL, L' and bpy = 4,4'-dicarboxy-2,2'-bipyridine, 5,5'-dicarboxy-2,2'-bipyridine and 2,2'-bipyridine, respectively.

^bFrom [10].

^cFrom [13].

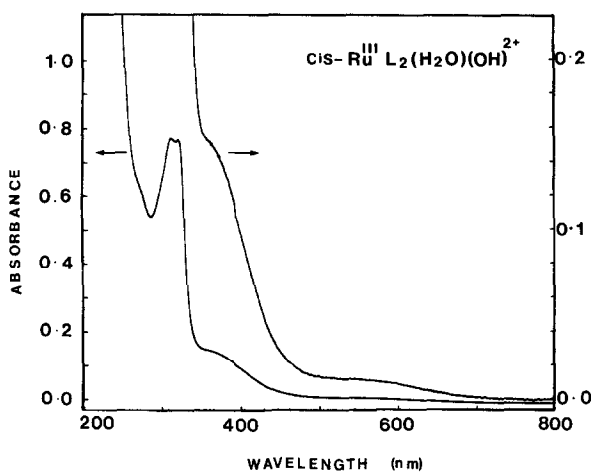
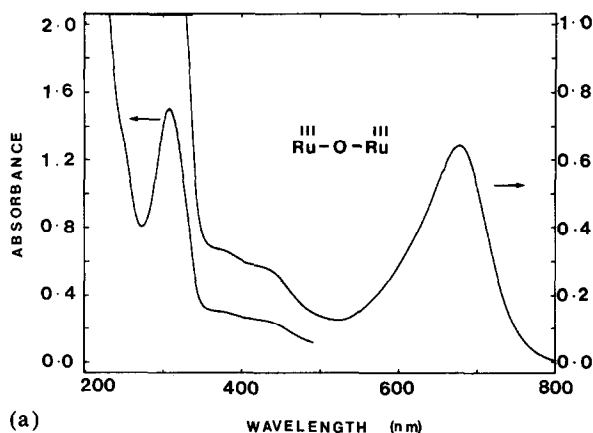


Fig. 3. Absorption spectrum of 3×10^{-5} M $[\text{cis-Ru}^{\text{III}}\text{L}_2(\text{H}_2\text{O})_2]^{\text{3+}}$ in 1 M $\text{CF}_3\text{SO}_3\text{H}$; 1 cm optical pathlength.

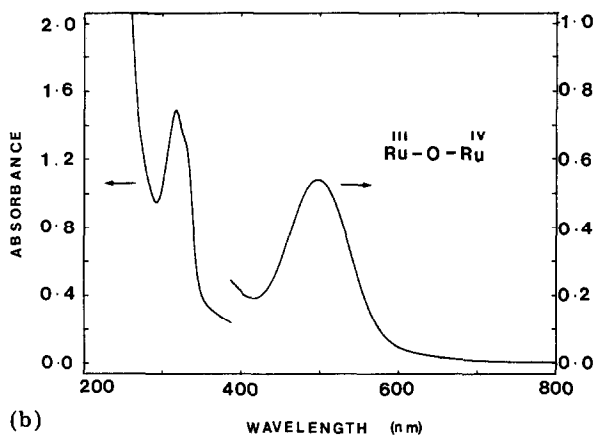
less than 5% of its initial value. The solution color had changed from red to faint yellow. The absorption spectrum (Fig. 3) shows maxima at 317 nm ($\epsilon = 2.2 \times 10^4 \text{ M}^{-1} \text{ cm}^{-1}$), 327 nm ($\epsilon = 2.2 \times 10^4 \text{ M}^{-1} \text{ cm}^{-1}$) and shoulders at about 280 and 370 nm. The spectral features of the 5,5'-dicarboxylated $\text{cis-Ru}^{\text{III}}\text{L}'_2(\text{H}_2\text{O})_2^{\text{3+}}$ analogue are similar (maxima at 314 and 326 nm), although additional peaks appear at 262 and 390 nm instead of the shoulders observed in Fig. 3.

Spectral characterization of $\text{L}_2(\text{H}_2\text{O})\text{Ru}-\text{O}-\text{Ru}(\text{H}_2\text{O})\text{L}_2$

The dimeric complex $\text{Ru}^{\text{III}}-\text{O}-\text{Ru}^{\text{III}}$ (for convenience, the dimer in its various oxidation states will be denoted by abbreviated formulas) was obtained by controlled electrolysis of $\text{cis-Ru}^{\text{II}}\text{L}_2(\text{H}_2\text{O})_2^{\text{2+}}$ solutions in 0.5 M H_2SO_4 and subsequent precipitation as the sulfate salt, as described in the experimental section. The spectrum obtained for the dimer in 1 M $\text{CF}_3\text{SO}_3\text{H}$ shows four absorption peaks located at 304 nm ($\epsilon = 4.9 \times 10^4 \text{ M}^{-1} \text{ cm}^{-1}$),



(a)



(b)

Fig. 4. (a) Absorption spectrum of 3×10^{-5} M $[\text{L}_2(\text{H}_2\text{O})\text{Ru}^{\text{III}}-\text{O}-\text{Ru}^{\text{III}}(\text{H}_2\text{O})\text{L}_2](\text{SO}_4)_2$ in 1 M aqueous $\text{CF}_3\text{SO}_3\text{H}$; 1 cm optical pathlength. (b) Absorption spectrum of 2.9×10^{-5} M $(\text{L}_2(\text{H}_2\text{O})\text{Ru}^{\text{III}}-\text{O}-\text{Ru}^{\text{IV}}(\text{H}_2\text{O})\text{L}_2)(\text{SO}_4)_2$ in 1 M aqueous $\text{CF}_3\text{SO}_3\text{H}$; 1 cm optical pathlength.

371 nm ($\epsilon = 1.2 \times 10^4 \text{ M}^{-1} \text{ cm}^{-1}$), 418 nm ($\epsilon = 1.0 \times 10^4 \text{ M}^{-1} \text{ cm}^{-1}$), and 678 nm ($\epsilon = 2.1 \times 10^4 \text{ M}^{-1} \text{ cm}^{-1}$), Fig. 4(a). The prominent feature in the visible region at 678 nm is responsible for the intense green coloration of the complex. In Table 3, we compare the spectral properties of $\text{Ru}^{\text{III}}-\text{O}-\text{Ru}^{\text{III}}$ to those of related dimers with carboxylic acid groups in the 5,5'-positions and without substituents. The unsubstituted dimer has a maximum at 637 nm below pH 5, whereas the 5,5'-dicarboxylated isomer has an adsorption peak at 650 nm.

The absorption in the red of μ -oxo ruthenium complexes with bipyridyl ligands has been attributed [16] to excitation of $d\Pi(\text{Ru})-p\Pi(\text{O})-d\Pi(\text{Ru})$ valence electrons involved in the formation of $\text{Ru}-\text{O}-\text{Ru}$ bonds. This assignment was based on a qualitative molecular orbital model developed by Dunitz and Orgel [17] for $\text{Cl}_5\text{Ru}-\text{O}-\text{RuCl}_5^{4-}$. However, metal-to-ligand

TABLE 3

UV-Vis spectral data of oxo-bridged ruthenium(III) dimer $[L_2(H_2O)Ru^{III}-O-Ru^{III}(OH_2)L_2](SO_4)_2$ and related complexes

Complex	Medium	λ_{max} (nm)	ϵ ($M^{-1} cm^{-1}$)
$[L_2(OH_2)Ru^{III}-O-Ru^{III}(OH_2)RuL_2](SO_4)_2$	1 M HCF_3SO_3	678	2.1×10^4
		418	9.9×10^3
		371	1.1×10^4
		304	4.9×10^4
$[L'_2(OH_2)Ru^{III}-O-Ru^{III}(OH_2)L'_2](SO_4)_2$	0.5 M H_2SO_4	654	1.8×10^4
		296	7.0×10^4
		275	5.5×10^4
$[(bpy)_2OH_2Ru^{III}-O-Ru^{III}(OH_2)(bpy)_2](ClO_4)_4$	pH 1	637	2.1×10^4
		280	5.03×10^4
		271	3.98×10^4

^aL, L' and bpy = 4,4'-dicarboxy-2,2'-bipyridine, 5,5'-dicarboxy-2,2'-bipyridine and 2,2'-bipyridine, respectively.

^bFrom [10].

^cFrom [9b].

charge transfer transitions could also contribute to the visible absorption, which renders its definite assignment difficult. The results in Table 3 indicate that the position of the maximum is sensitive to the energy of the ligand Π^* orbital, which decreases in the order $bipy > L' > L$. The absorption maximum of the dimers shifts to longer wavelengths as the energy of the ligand orbital decreases. This implies that the optical transition involves either charge transfer from the Ru—O—Ru bridge to the ligand or that the Ru—O—Ru Π^* levels decrease as the Ru back-bonding to the ligand increases.

The absorption of Ru—O—Ru in the red spectral region is dependent on pH, as displayed in Fig. 5. Between pH 0 and 1, λ_{max} decreases from 678 to 668 nm, where it remains until pH 5. A further significant blue shift to 640 nm occurs between pH 5 and 8. This is followed by an increase in λ_{max} to 648 nm in more alkaline solution. Apart from the displacement of the maximum, there is significant broadening of the absorption peak. Thus, at pH 9 (0.1 M carbonate buffer) the extinction coefficient at the maximum is $1.4 \times 10^4 M^{-1} cm^{-1}$. These spectral changes arise from the various acid-base equilibria involving the two H_2O ligands and the peripheral COOH substituents of the dimer. There are 8 carboxylic acid groups that should be fully dissociated at the pH > 4, assuming that their acidity is similar to that of the monomer $Ru^{III}L_2(H_2O)(OH)$. The dissociation of these substituents brings about the blue shift observed in acidic solution. Therefore, it is reasonable to assign the spectral changes above pH 5 to the dissociation of the water ligands, yielding pK_a values of 6.2 ± 0.2 and 8.5 ± 0.4 , respectively. The pK_a values for $(bpy)_2(H_2O)Ru^{III}-O-Ru^{III}(H_2O)(bpy)_2$ have been determined as 5.9 and 8.3, which are similar to those of the carboxylated dimer.

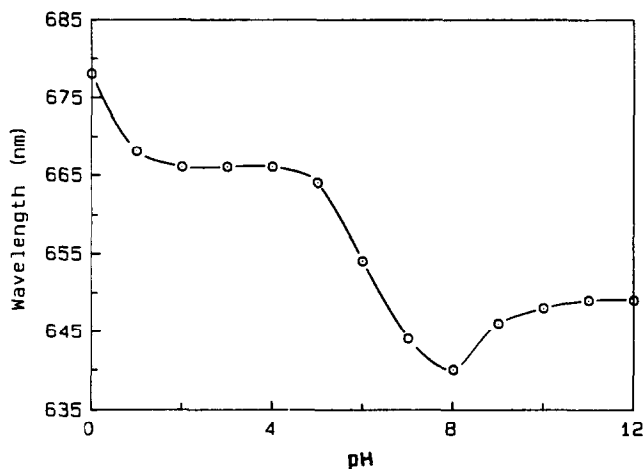


Fig. 5. Effect of pH on the absorption maximum of $L_2(H_2O)Ru^{III}-O-Ru^{III}(H_2O)L_2$ in the red wavelength region.

The UV-visible absorption spectrum of the mixed-valence dimer $Ru^{III}-O-Ru^{IV}$ was obtained from solutions prepared by chemical oxidation of $Ru^{III}-O-Ru^{III}$. Cobaltic ions produced by electrolysis of Co^{2+} in CF_3SO_3H [10] were used under acidic conditions. A solution of $2.9 \times 10^{-5} M$ $Ru^{III}-O-Ru^{III}$ in $1 M$ CF_3SO_3H was mixed with a slight stoichiometric excess of Co^{3+} , resulting in an immediate color change from blue-green to red. The absorption spectrum of the product in Fig. 4(b) shows a symmetric peak at $500 nm$ ($\epsilon = 1.8 \times 10^4 M^{-1} cm^{-1}$). The spectrum is red-shifted with respect to the unsubstituted analogue, $(bpy)_2(H_2O)Ru^{III}-Ru^{IV}(bpy)_2(H_2O)$. In the visible region, the unsubstituted dimer is very similar to that of the isomeric 5,5'-carboxylated mixed-valence dimer $L'(H_2O)Ru^{III}-O-Ru^{IV}(H_2O)L'$, which also has a peak at $500 nm$ ($\epsilon = 1.7 \times 10^4 M^{-1} cm^{-1}$) [10].

In alkaline solution, the conversion of $Ru^{III}-O-Ru^{III}$ to the mixed-valence dimer was carried out using peroxodisulfate or H_2O_2 as an oxidant. Figure 6 shows spectral changes resulting from the addition of $10^{-2} M$ $Na_2S_2O_8$ to a $5 \times 10^{-5} M$ solution of $Ru^{III}-O-Ru^{III}$ in $5 \times 10^{-2} M$ $NaHCO_3$ buffer (pH 9.3). The time interval between each successive recording of the solution spectrum was 6 min. Initially, the prominent peak of $Ru^{III}-O-Ru^{III}$ (centered at $648 nm$) is present, which converts quantitatively within 1 h to that of $Ru^{III}-O-Ru^{IV}$. Spectral maxima are at $500 nm$ ($\epsilon = 2 \times 10^4 M^{-1} cm^{-1}$), $308 nm$ ($\epsilon = 5 \times 10^4 M^{-1} cm^{-1}$), and a shoulder at $360 nm$. Comparison with the spectrum of $Ru^{III}-O-Ru^{IV}$ in $1 M$ CF_3SO_3H , Fig. 4(b), shows that the effect of pH on the absorption features of the mixed-valence dimer is small.

Electrochemical characterization of $L_2(H_2O)Ru^{III}-O-Ru^{III}(H_2O)L_2$

Figure 7(a) shows a cyclic voltammogram of a solution containing $5 \times 10^{-5} M$ $Ru^{III}-O-Ru^{III}$ and $1 M$ CF_3SO_3H in the potential range 0.5 to $1.5 V$.

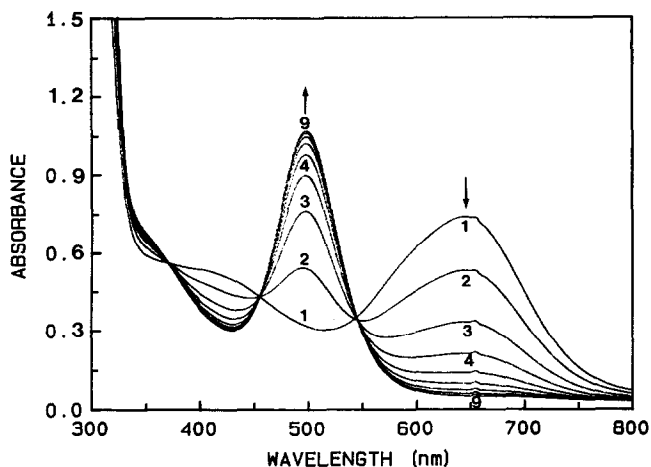
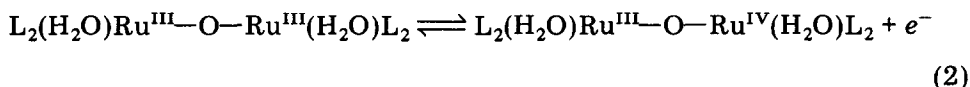
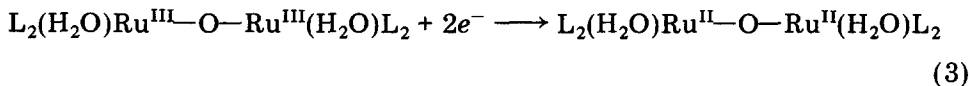


Fig. 6. Visible absorption spectrum of 5×10^{-5} M $\text{Ru}^{\text{III}}\text{—O—Ru}^{\text{III}}$ in 5×10^{-2} M NaHCO_3 buffer, pH 9.3. Conversion to mixed-valence dimer using 1×10^{-2} M $\text{Na}_2\text{S}_2\text{O}_8$ as oxidant. Time interval between each recording after addition of $\text{Na}_2\text{S}_2\text{O}_8$ is 6 min.

It is distinguished by a reversible one-electron wave (peak separation 60 mV), centered at 0.9 V, corresponding to the oxidation of $\text{Ru}^{\text{III}}\text{—O—Ru}^{\text{III}}$ to the mixed-valence dimer. Assuming that the diffusion and activity coefficients of $\text{Ru}^{\text{III}}\text{—O—Ru}^{\text{III}}$ and $\text{Ru}^{\text{III}}\text{—O—Ru}^{\text{IV}}$ are the same, the mid-point potential corresponds to the standard potential of the redox equilibrium:



The value of $E^0 = 0.9$ V (SCE) derived from Fig. 7(a) is 0.1 V more positive than that of the unsubstituted dimer, but 0.1 V more negative than the E^0 for the isomeric analogue with carboxylic acid groups in the 5,5'-position. At potentials positive of 1.2 V, there is a pronounced catalytic wave arising from water oxidation. (In the absence of dimer, the current in the entire potential range remained below $1 \mu\text{A}$.) If the potential is scanned from 0.5 to 0 V (scan rate 50 mV s^{-1}), one observes a cathodic wave with a maximum at 0.26 V. The corresponding anodic peak at *ca.* 0.4 V is barely visible during the reverse scan, indicating that the redox process is chemically irreversible on a time scale of 10 s. The cathodic wave at 0.26 V is assigned to the two-electron reduction of $\text{Ru}^{\text{III}}\text{—O—Ru}^{\text{III}}$.



In 1 M $\text{CF}_3\text{SO}_3\text{H}$, the $\text{Ru}^{\text{II}}\text{—O—Ru}^{\text{II}}$ is unstable towards hydrolysis and undergoes fragmentation into two molecules of *cis*- $\text{Ru}^{\text{II}}\text{L}_2(\text{H}_2\text{O})_2$:



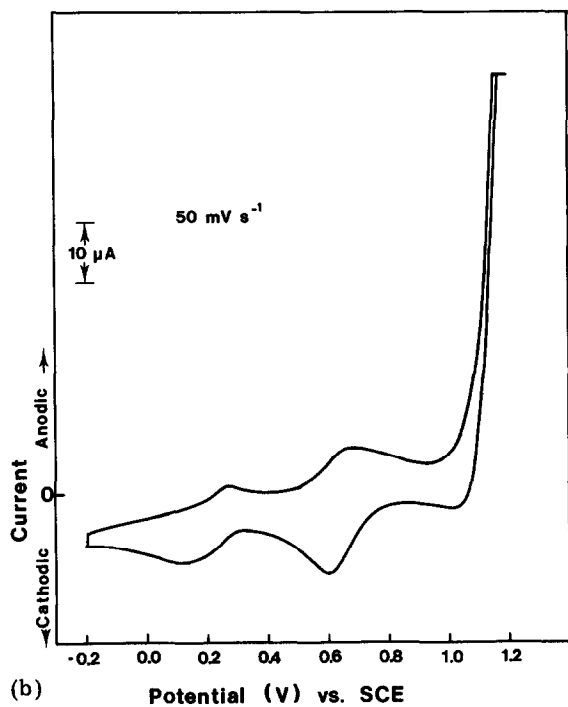
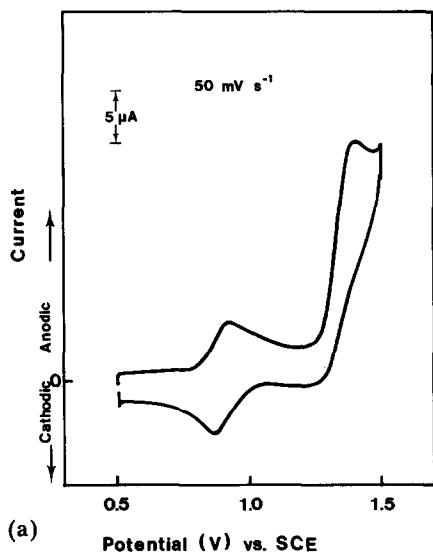


Fig. 7. (a) Cyclic voltammogram of $5 \times 10^{-5} \text{ M}$ $[\text{L}_2(\text{H}_2\text{O})\text{Ru}^{\text{III}}-\text{O}-\text{Ru}^{\text{III}}(\text{H}_2\text{O})\text{L}_2](\text{SO}_4)_2$ in aqueous 1 M $\text{CF}_3\text{SO}_3\text{H}$ In-doped SnO_2 working electrode (1 cm^2 area). (b) Cyclic voltammogram of $5 \times 10^{-5} \text{ M}$ $[\text{L}_2(\text{H}_2\text{O})\text{Ru}^{\text{III}}-\text{O}-\text{Ru}^{\text{III}}(\text{H}_2\text{O})\text{L}_2](\text{SO}_4)_2$ in aqueous 1 M LiCF_3SO_3 , pH 3.25, solution contains $2.5 \times 10^{-3} \text{ M}$ MES buffer; In-doped SnO_2 working electrode (1 cm^2 area).

Reactions (3) and (4) are confirmed by the formation of *cis*-RuL₂(H₂O)₂ upon electrolysis of Ru^{III}-O-Ru^{III} solutions in 1 M CF₃SO₃H. Coulometric analysis showed that two electrons are consumed in the reduction of one Ru^{III}-O-Ru^{III} molecule.

Reductive cleavage has been observed with other dimers, *i.e.* (bpy)₂-(H₂O)Ru^{III}-O-Ru^{III}(H₂O)(bpy)₂ [9] and the analogous osmium complex (bpy)₂(H₂O)Os^{III}-O-Os^{III}(H₂O)(bpy)₂ [18]. Hydrolysis and splitting of the μ -oxo bridge was found to be greatly accelerated with decreasing pH. At pH \leq 5 for the ruthenium and pH \leq 3 for the osmium complex, the breakdown of the dimer was sufficiently rapid that the III-III \rightarrow II-II reduction became chemically irreversible at a scan rate of 200 mV s⁻¹. The instability of the μ -oxo-bridge in the Ru dimer is also observed when carboxylated groups are introduced in the 5,5'-position of the bipyridyl ligand, making the complex sensitive to reductive cleavage, in acid solution.

Our present findings with L₂(H₂O)Ru^{III}-O-Ru^{III}(H₂O)L₂ stand in striking contrast to this behavior. Figure 7(a) shows a cyclic voltammogram obtained with 5×10^{-5} M L₂(H₂O)Ru^{III}-O-Ru^{III}(H₂O)L₂ at pH 3.25. Here, the reduction of Ru^{III}-O-Ru^{III} is chemically reversible, with no reductive cleavage being observed on the time scale of cyclic voltammetry. The reductive peak has shifted to 0.1 V, and there is a distinct anodic peak at 0.26 V, yielding $E_{1/2} = 0.18$ V. (Because the peak separation is larger than the value of 29 mV expected for a two-electron process, the heterogeneous charge transfer reaction (3) must be slow at the SnO₂/In₂O₃-electrolyte interface, resulting in quasi-reversible electrochemical behavior.) Apparently, substitution of the bpy ligands with carboxylate groups in the 4,4'-position greatly enhances the stability of the Ru^{II}-O-Ru^{II} dimer in acidic solution. The opposite effect is observed when the COOH substituents are introduced in 5,5'-positions. Here, the reduction of the III-III dimer is chemically irreversible at pH 3.25. This finding illustrates that a small change in the position of a peripheral substituent can have a dramatic effect on the chemical stability of the oxo-bridged dimer.

Apart from the reduction of Ru^{III}-O-Ru^{III}, one observes in Fig. 7(b) a second wave centered at 630 mV, corresponding to the reversible one-electron oxidation of the dimer. In addition, a catalytic wave arising from water oxidation to oxygen is observed, starting at 100 to 200 mV positive of the reversible O₂ evolution potential.

Figure 8 presents the effect of pH on the $E_{1/2}$ values for both the oxidation and reduction of Ru^{III}-O-Ru^{III} in a Pourbaix-type diagram. The stable oxidation states of the dimer expressed with Roman numerals are indicated as a function of solution potential and pH. The upper limit of stability of the mixed-valence dimer Ru^{II}-O-Ru^{IV} corresponds approximately to the onset of the catalytic wave, situated 100 to 200 mV positive of the reversible oxygen evolution potential. The latter is indicated with a dashed line. The two vertical lines in the diagram indicate the pK values for the two water ligands of Ru^{III}-O-Ru^{III}. Since the one-electron oxidation of Ru^{III}-O-Ru^{III} is electrochemically reversible, $E_{1/2}$ is equal to the standard redox potential E^0 ,

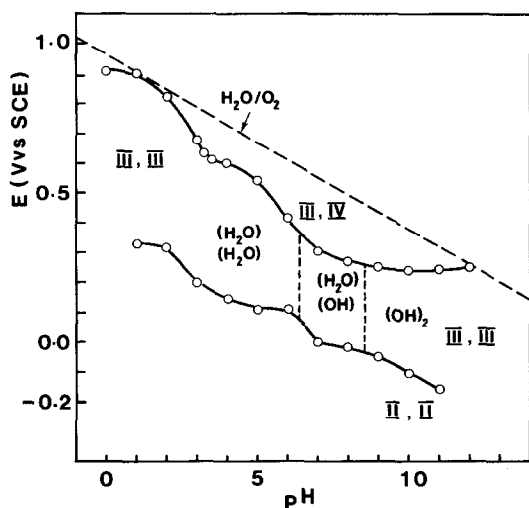
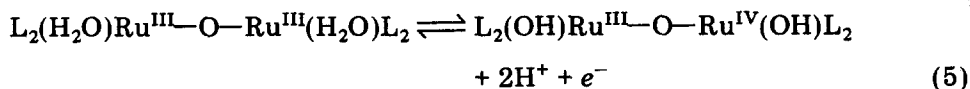


Fig. 8. Pourbaix diagram for the μ -oxo dimer, pH dependence of $E_{1/2}$ values vs. SCE measured by cyclic voltammetry for $[\text{L}_2(\text{H}_2\text{O})\text{Ru}^{\text{III}}-\text{O}-\text{Ru}^{\text{III}}(\text{H}_2\text{O})\text{L}_2]^{4+}$. The oxidation states of the metal sites in the various pH-potential domains are indicated by Roman numerals. The protonation states of the two water ligands are indicated by abbreviations such as $(\text{H}_2\text{O})(\text{OH})$. The vertical lines correspond to pK_a values of the two water ligands in the III,III oxidation states. The dashed line indicates the reversible water oxidation potential.

provided the diffusion coefficients in the reduced and oxidized states are the same. On the other hand, thermodynamic interpretation of the $E_{1/2}$ values observed for the $\text{Ru}^{\text{III}}-\text{O}-\text{Ru}^{\text{IV}}/\text{Ru}^{\text{III}}-\text{O}-\text{Ru}^{\text{III}}$ couple should be made with caution, since in this case quasi-reversible electrochemical behavior was observed. This implies that the position of the cathodic and anodic peaks depends on kinetic parameters, and their average value $E_{1/2}$ may not be identical with E^0 .

Focusing attention first on the $\text{Ru}^{\text{III}}-\text{O}-\text{Ru}^{\text{IV}}/\text{Ru}^{\text{III}}-\text{O}-\text{Ru}^{\text{III}}$ redox equilibrium, the E^0 value decreases sharply from 0.9 V at pH 1 to 0.6 V at pH 4. This pH effect is probably associated with the deprotonation of one or both water ligands of the mixed-valence dimer. The fact that the 8 peripheral COOH groups undergo dissociation in the same pH region prevents us from giving a more detailed interpretation. Interestingly, in the pH domain between 5 and 7, the slope of the curve is -120 mV/pH , indicating a $1e^-/2\text{H}^+$ process. This concurs with $\text{Ru}^{\text{III}}-\text{O}-\text{Ru}^{\text{III}}$ having two undissociated aqua ligands, while in the mixed-valence state both are deprotonated:



Above pH 7 the slope decreases, as expected from the pK values of the III-III dimer. A potential of 0.23 V is reached at pH 10. No further changes

occur at higher pH, indicating that in both the oxidized and reduced states the dimer has two hydroxy ligands:



The E^0 values for the $Ru^{III}-O-Ru^{III}/Ru^{III}-O-Ru^{IV}$ couple at pH 5 are very similar to those of the unsubstituted dimer $(bpy)_2(H_2O)Ru^{III}-O-Ru^{III}(H_2O)(bpy)_2$. This indicates that the carboxylate groups exert a much smaller effect on the redox equilibrium of the III-III and III-IV dimers than undissociated carboxylic acid substituents. A similar trend was observed in the case of RuL_3 . The E^0 value is 1.32 V for the complex with carboxylic acid groups in the 4,4'-position of the bipyridyl ligand, decreasing to 1 V upon deprotonation of the COOH groups. The latter is practically the same as E^0 for the $Ru(bpy)_3^{2+/3+}$ couple. These findings are readily understood in terms of the much stronger electron-withdrawing power of the COOH as compared to the CO_2^- groups, lowering the electron density on the Ru center.

Considering next the reduction of $Ru^{III}-O-Ru^{III}$, it is apparent from Fig. 8 that the $E_{1/2}$ value decreases also with increasing pH but to a smaller degree than E^0 for the oxidation. The change from 0.32 to 0.2 V occurring between pH 2 and 3 is associated with the deprotonation of the carboxylic acid ligands. This is followed by a plateau up to pH 6. Between pH 6 and 11, the decrement of $E_{1/2}$ is -56 mV/pH, which is close to the -59 mV/pH expected for a $1e/1H$ or a $2e/2H$ process.

Sulfato-complex formation of the mixed-valence dimer $Ru^{III}-O-Ru^{IV}$

In analogy to the 5,5'-carboxylated isomer [10], the complex $L_2(H_2O)-Ru^{III}-O-Ru^{IV}(H_2O)L_2$ in 0.5 M sulfuric acid undergoes replacement of water ligands by sulfate or bisulfate anions. This has a pronounced effect on the redox properties of the dimer. The cyclic voltammogram obtained from a 5×10^{-4} M solution of $Ru^{III}-O-Ru^{IV}$ in 0.5 M H_2SO_4 is shown in Fig. 9(a). It exhibits a quasi-reversible wave (70 mV peak separation) centered at 755 mV, a small shoulder around 900 mV and the onset of a catalytic wave at potentials more positive than 1.3 V at a scan rate of 50 mV s^{-1} . These features are strikingly different from the cyclic voltammogram obtained with $Ru^{III}-O-Ru^{IV}$ in 1 M CF_3SO_3H , which shows a reversible wave at 0.9 V. The wave observed at 0.725 V in sulfuric acid solutions arises from a sulfato complex of $Ru^{III}-O-Ru^{IV}$. Different structures are possible, since sulfate can coordinate to the Ru centers as a mono- or bidentate ligand. Furthermore, complexation by bisulfate can also occur.

Interestingly, the sulfato complex becomes unstable upon reduction of the III-IV to the III-III redox state. In Fig. 9(b) is shown a cyclic voltammogram obtained after electrolysis of the $Ru^{IV}-O-Ru^{III}$ solution at 0.65 V until nearly complete conversion to $Ru^{III}-O-Ru^{III}$. The main wave is now centered at 0.9 V, as in Fig. 7(a) for the solution of $Ru^{III}-O-Ru^{III}$ in CF_3SO_3H , the hump of the sulfato complex around 0.7 V being barely visible. The catalytic wave is now much more pronounced, the anodic

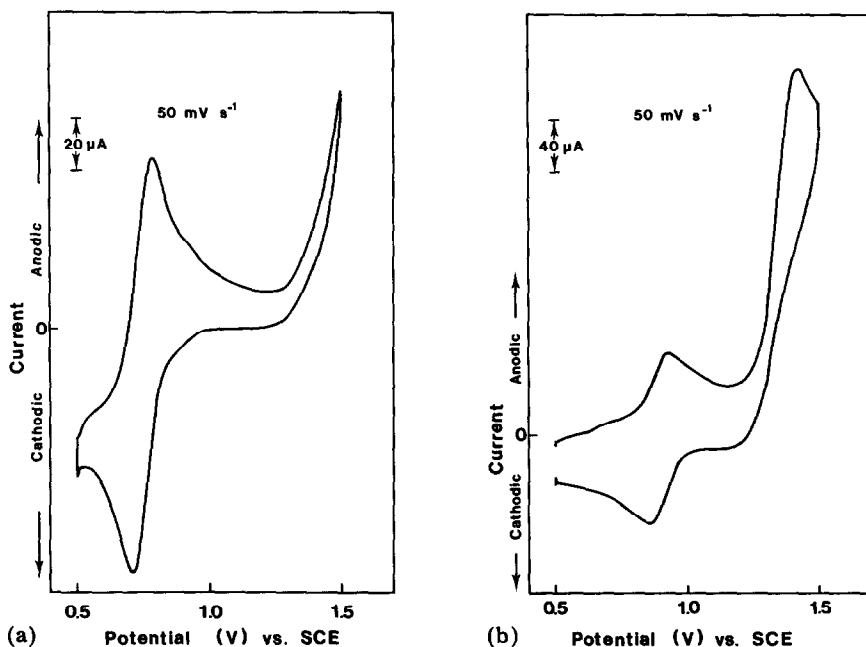


Fig. 9. Cyclic voltammograms of 5×10^{-4} M Ru-O-Ru in 0.5 M H_2SO_4 ; In-doped SnO_2 working electrode, 1 cm^2 area. (a) Solution contains sulfato complexes of $\text{Ru}^{\text{III}}\text{-O-Ru}^{\text{IV}}$; (b) after solution (a) was kept at 0.65 V until nearly complete conversion of $\text{Ru}^{\text{III}}\text{-O-Ru}^{\text{IV}}$ to $\text{Ru}^{\text{III}}\text{-O-Ru}^{\text{III}}$.

current rising steeply at potentials exceeding 1.2 V. The difference in the cyclic voltammograms obtained prior and subsequent to reduction are attributed to the replacement of sulfate or bisulfate by water ligands upon conversion of $\text{Ru}^{\text{III}}\text{-O-Ru}^{\text{IV}}$ to $\text{Ru}^{\text{III}}\text{-O-Ru}^{\text{III}}$. Presumably, the high electrophilicity of the Ru centers in the mixed-valence state favors sulfate coordination. Upon reduction, the $d(\text{II})\text{Ru}$ density is increased, leading to the exchange of sulfate with H_2O . From the fact that two distinctly different voltammograms are obtained for $\text{Ru}^{\text{III}}\text{-O-Ru}^{\text{IV}}$ and $\text{Ru}^{\text{III}}\text{-O-Ru}^{\text{III}}$, it can be inferred that the ligand replacement reaction is slow on the time scale of cyclic voltammetry. Similar effects were observed with the 5,5'-carboxylated dimer [10].

A behavior that distinguishes $\text{Ru}^{\text{III}}\text{-O-Ru}^{\text{III}}$ from the analogous dimer carboxylated in the 5,5'-position of the bipyridyl ligands is the low solubility of its sulfate salt in acid solution. This greatly facilitates the isolation and purification of this complex.

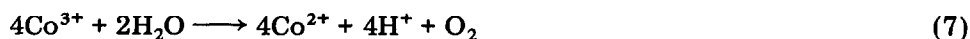
Water oxidation catalysis

The cyclic voltammograms in Figs. 7 - 9 show large catalytic waves with an onset *ca.* 200 mV positive of the reversible oxygen evolution potential. The appearance of the high anodic current close to the thermodynamic threshold signifies efficient water oxidation catalysis by the carboxylated

ruthenium dimer. The kinetics for the catalytic oxidation of water with the carboxylated dimer are more favorable than with $(\text{bpy})_2(\text{H}_2\text{O})\text{Ru}^{\text{III}}-\text{O}-\text{Ru}^{\text{III}}(\text{H}_2\text{O})(\text{bpy})_2$. The latter shows no catalytic wave for the oxidation of water on a glassy carbon electrode at scan rates of 50 mV s^{-1} , indicating sluggish water oxidation kinetics. The intervention of $\text{L}_2(\text{H}_2\text{O})\text{Ru}^{\text{III}}-\text{O}-\text{Ru}^{\text{III}}(\text{H}_2\text{O})\text{L}_2$ as an efficient water oxidation catalyst is corroborated by the following results from chemical and photochemical oxygen evolution experiments.

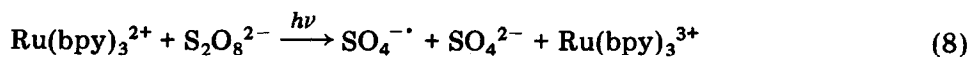
Dropwise addition of a $2.8 \times 10^{-2} \text{ M Co}^{3+}$ solution in 3 M HClO_4 to $10 \text{ ml } 1 \text{ M CH}_3\text{SO}_3\text{H}$ solution containing $1 \times 10^{-7} \text{ mol Ru}^{\text{III}}-\text{O}-\text{Ru}^{\text{III}}$ resulted in the immediate appearance of the characteristic red color of the mixed-valence dimer. The spectrum of $\text{Ru}^{\text{III}}-\text{O}-\text{Ru}^{\text{IV}}$ persisted even after the addition of a 140-fold stoichiometric excess of Co^{3+} . The excess Co^{3+} ions were rapidly reduced to Co^{2+} with the simultaneous evolution of oxygen. The generation of O_2 was monitored quantitatively with a Clark-type sensor mounted in the head space of the cell, and the data were confirmed by gas chromatography.

Oxygen evolution proceeded at a rate of $30 \mu\text{l (STP) h}^{-1}$, while in the absence of $\text{Ru}^{\text{III}}-\text{O}-\text{Ru}^{\text{IV}}$ the rate was $0.45 \mu\text{l h}^{-1}$. Thus, 10^{-7} mol of dimer are sufficient to accelerate 66-fold the water oxidation rate by Co^{3+} . The reaction came near to completion after a few hours when $80 \mu\text{l}$ of O_2 had been produced, corresponding to 33 turnovers of the complex. The amount of O_2 evolved and Co^{3+} reduced correspond to the stoichiometry of the process:

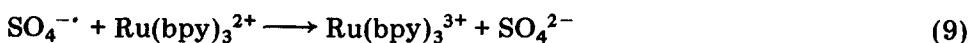


After complete conversion of Co^{3+} to Co^{2+} in the water oxidation reaction, the spectral features of the solution showed the presence of $\text{Ru}^{\text{III}}-\text{O}-\text{Ru}^{\text{IV}}$ with a small contribution of $\text{Ru}^{\text{III}}-\text{O}-\text{Ru}^{\text{III}}$, the total concentration of dimer being *ca.* $6 \times 10^{-6} \text{ M}$. This indicates that 40% degradation of the catalyst had occurred during the oxygen evolution process. Under similar conditions, the 5,5'-carboxylated dimer showed no decomposition after 75 turnovers. Thus, in the strongly oxidizing environment prevailing in acidic Co^{3+} solutions ($E > 1.5 \text{ V}$), the stability of the dimer with 4,4'-COOH substituents appears to be inferior to that with carboxylic acid groups in the 5,5'-position.

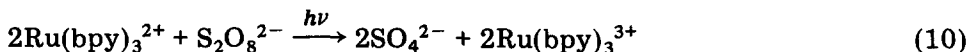
Visible light-induced generation of oxygen was assayed using $\text{Ru}(\text{bpy})_3^{2+}$ as a sensitizer and peroxodisulfate as a sacrificial electron acceptor. The excited state of $\text{Ru}(\text{bpy})_3^{2+}$ is oxidatively quenched by the $\text{S}_2\text{O}_8^{2-}$, the rate constant for the electron transfer [18, 19] being $8 \times 10^8 \text{ M}^{-1} \text{ s}^{-1}$.



Because the $\text{SO}_4^{\cdot-}$ radical oxidizes a second $\text{Ru}(\text{bpy})_3^{2+}$:



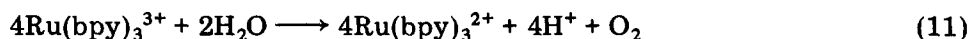
the overall light reaction is:



Irradiation of 10 ml solution containing 10^{-4} M $\text{Ru}(\text{bpy})_3^{2+}$, 5×10^{-3} M sodium peroxodisulfate and 0.1 M bicarbonate buffer (pH 9) with the $\lambda > 455$ nm output of a 150 W tungsten-halogen lamp resulted in rapid bleaching of the sensitizer. Spectral analysis shows the appearance of absorption maxima at 448 and 628 nm. These features are attributed to the dimers $(\text{bpy})_2(\text{HO})\text{Ru}^{\text{III}}-\text{O}-\text{Ru}^{\text{IV}}(\text{HO})(\text{bpy})_2$ and $(\text{bpy})_2(\text{OH})\text{Ru}^{\text{III}}-\text{O}-\text{Ru}^{\text{III}}(\text{OH})(\text{bpy})_2$ formed under illumination. Using literature extinction coefficients [19], concentration of the dimers was determined as 1.4×10^{-5} M and 6×10^{-6} M, respectively. Based on the initial $\text{Ru}(\text{bpy})_3^{2+}$ concentration, this corresponds to 40% conversion.

The formation of $(\text{bpy})_2(\text{OH})\text{Ru}^{\text{III}}-\text{O}-\text{Ru}^{\text{III}}(\text{OH})(\text{bpy})_2$ in alkaline solutions of $\text{Ru}(\text{bpy})_3^{3+}$ has already been discussed by Lay and Sasse [20]. The mechanism suggested involves nucleophilic attack of water on the metal to form a 7-coordinate intermediate followed by oxidation, loss of one ligand and dimerization. It was proposed that the dimer plays the role of a catalyst in the oxidation of water by $\text{Ru}(\text{bpy})_3^{3+}$, which at pH 9 occurs spontaneously [21], albeit with a very small yield [22]. Our results support such a mechanism.

In Fig. 10 the amount of oxygen present in the head space of the vessel is plotted as a function of illumination time. In the absence of $\text{L}_2(\text{OH})\text{Ru}^{\text{IV}}-\text{O}-\text{Ru}^{\text{III}}(\text{OH})\text{L}_2$, there is an induction period of 20 min during which O_2 generation is negligible. Thereafter, the O_2 level increases, until after 70 min of photolysis a plateau is reached where ca. 20 μl of oxygen have been produced. Presumably, part of the $\text{Ru}(\text{bpy})_3^{3+}$, generated under light via reaction (10), is converted to $(\text{bpy})_2(\text{OH})\text{Ru}^{\text{IV}}-\text{O}-\text{Ru}^{\text{III}}(\text{OH})(\text{bpy})_2$, which, in turn, catalyzes oxidation of water by the remaining fraction of the sensitizer:



In the presence of $\text{L}_2(\text{OH})\text{Ru}^{\text{IV}}-\text{O}-\text{Ru}^{\text{III}}(\text{OH})\text{L}_2$, there is no induction period and the photogeneration of oxygen is greatly enhanced, as shown in Figs. 10(a) and 10(b). Maximal rates of O_2 production are 24, 224 or 454 $\mu\text{l h}^{-1}$ in the absence and presence of 0.1 or 0.2 μmol of $\text{L}_2(\text{OH})\text{Ru}^{\text{IV}}-\text{O}-\text{Ru}^{\text{III}}(\text{OH})\text{L}_2$, respectively. Formation of oxygen bubbles under illumination is readily visible in solutions containing the carboxylated $\text{Ru}^{\text{III}}-\text{O}-\text{Ru}^{\text{IV}}$.

The photolysis experiment in Fig. 10 was stopped after 2 h. At this time, 5 or 10 μmol oxygen had been produced with the solutions containing 0.1 or 0.2 μmol $\text{Ru}^{\text{III}}-\text{O}-\text{Ru}^{\text{IV}}$, respectively. Therefore, the turnover number in both experiments is 50. Because there are 50 μmol peroxodisulfate present, at most 25 μmol O_2 can be generated. Hence, the yield in experiment (b) is 40% of theoretical value after 2 h of photolysis. The gradual decline in the rate of O_2 formation during illumination is due to depletion

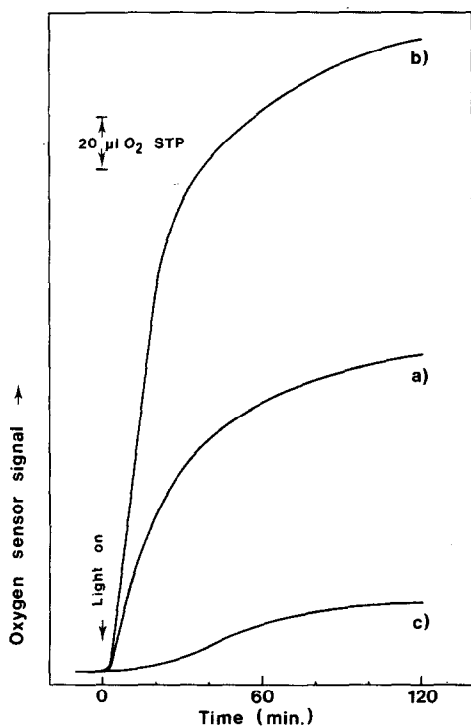


Fig. 10. Visible light-induced oxygen generation with solutions containing 1×10^{-4} M $\text{Ru}(\text{bipy})_3^{2+}$ as a sensitizer, 5×10^{-3} M $\text{Na}_2\text{S}_2\text{O}_8$ as a sacrificial electron acceptor and 0.1 M sodium bicarbonate buffer, pH 9. 150 W tungsten halogen lamp, 455 nm cut-off filter, solution volume 10 ml thermostatted at 20 °C. (a) 1×10^{-7} mol $\text{Ru}^{\text{III}}\text{—O—Ru}^{\text{III}}$ added; (b) 2×10^{-7} mol $\text{Ru}^{\text{III}}\text{—O—Ru}^{\text{III}}$ added; (c) no dimer.

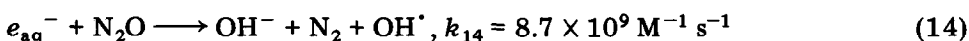
of the sensitizer, as shown by spectrophotometric analysis. The dimer is employed at too low a concentration to inhibit entirely the destructive side reactions of $\text{Ru}(\text{bpy})_3^{3+}$.

Mechanism of water oxidation catalysis, pulse radiolysis studies

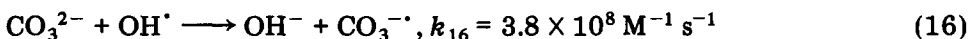
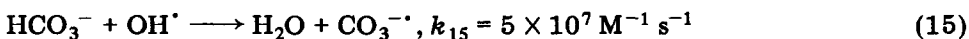
The intervention of the carboxylated dimer as a molecular water oxidation catalyst is a very rapid process, the catalytic current appearing close to the equilibrium potential for oxygen evolution. This renders difficult the electrochemical identification of the higher redox states of the dimer involved in the reaction. The situation is different for $(\text{bpy})_2(\text{H}_2\text{O})\text{Ru}^{\text{III}}\text{—O—Ru}^{\text{IV}}(\text{OH})(\text{bpy})_2$ which at a scan rate of 50 mV s^{-1} exhibits no catalytic wave for the oxidation of water on a glassy carbon electrode [9]. Consequently, the electrochemical characterization of the higher oxidation states of the unsubstituted dimer has been possible [9].

We report here for the first time on pulse radiolysis investigations aimed at identifying the nature and kinetics of short-lived redox states of the μ -oxo dimer that intervene in the water oxidation catalysis. Experiments

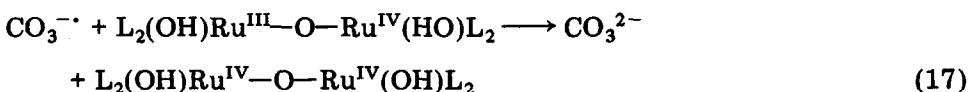
employed aqueous solutions of 43.9 - 96.4 μM $\text{L}_2(\text{H}_2\text{O})\text{Ru}^{\text{III}}\text{—O—Ru}^{\text{III}}(\text{H}_2\text{O})\text{L}_2$ containing 0.1 M NaHCO_3 (pH 9.15). Conditions are similar to those selected for visible light-induced oxygen evolution in Fig. 10. Prior to the experiments, the III-III dimer was quantitatively converted to the III-IV mixed-valence state by reaction with a four-fold stoichiometric excess of peroxodisulfate. Pulse radiolysis was carried out with a 3 MeV Van de Graaff accelerator, with the pulse width being 50 ns and the beam current for most of the experiments *ca.* 0.3 A. The equipment used for time-resolved spectroscopy has been described previously [23]. All solutions were saturated with N_2O . Under these conditions, the primary events occurring during the radiation pulse lead primarily to the formation of hydroxyl radicals (g value 5.4) apart from small yields of H^\cdot atoms and molecular products, *i.e.* H_2 ($g = 0.45$) and H_2O_2 ($g = 0.7$):



Under our conditions, the OH^\cdot radicals are efficiently scavenged by bicarbonate and carbonate ions leading to the formation of $\text{CO}_3^{\cdot-}$ anion radicals:



The latter are strong one-electron oxidants and abstract an electron from the mixed-valence dimer, producing the IV-IV oxidation state:



The time course of this process was followed by recording the bleaching of the 500 nm absorption of the III-IV dimer, Fig. 11. From the kinetic analysis of the absorption decrease, the rate constant for reaction (17) is derived to be $3.2 \times 10^7 \text{ M}^{-1} \text{ s}^{-1}$. The IV-IV state of the dimer is unstable and undergoes chemical transformations in the millisecond to second time domain, leading to the entire recovery of the initial absorption of the III-IV oxidation state. From the photochemical and electrochemical evidence presented in the previous chapters, there can be no doubt that water is the ultimate reductant in this transformation and oxygen is the reaction product. Unfortunately, during the reaction time of 0.01 to 1 s, diffusional displacement of intermediates from the part of the cell exposed to the electron beam to the unirradiated part of the solution occurred. This leads to changes in

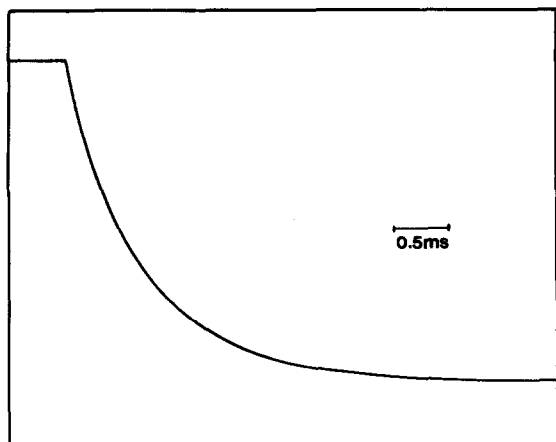


Fig. 11. Pulse radiolytic investigation of the oxidation of $\text{Ru}^{\text{III}}\text{-O-Ru}^{\text{IV}}$ by $\text{CO}_3^{\cdot-}$ radical ions. Time course of the bleaching of the 500 nm absorption conditions: NaHCO_3 0.1 M (pH 9.15), $\text{Ru}^{\text{III}}\text{-O-Ru}^{\text{IV}}$ concentration 4.4×10^{-5} M; $\text{Na}_2\text{S}_2\text{O}_8$ 5×10^{-4} M; solutions were deaerated with Ar and subsequently saturated with N_2O .

local concentration of the reactants, rendering meaningless kinetic analysis of the time course for the bleaching recovery. In any event, the conversion of IV-IV to IV-III dimer was complete within at most a few seconds and no degradation of dimer was noted upon repeated irradiation of the solution by electron pulses. This indicates that a truly catalytic cycle is operative in this system, contributions from reactions other than water oxidation by the IV-IV dimer being negligible.

These preliminary studies already provide information concerning the nature of the catalytic water oxidation cycle that is operative in this system. Apparently, the IV-IV state of the dimer formed by one-electron oxidation is unstable with respect to conversion of the III-IV redox state through water oxidation. Interestingly, a very recent paper by Raven and Meyer [24] reports that in the case of the oxo-bridged dimer with unsubstituted bipyridyl ligands, water is oxidized only by the higher valent IV-V dimer which has a lifetime of *ca.* 1 h in aqueous solution. Substitution of the ligands with carboxylate groups changes the redox and catalytic properties of the dimer in a dramatic fashion. This is evident from the present finding that water oxidation in the case of the carboxylated dimer occurs most likely already from the IV-IV oxidation state and at a rate that at least one thousand times faster than that observed with the IV-V oxidation state of the unsubstituted analogue.

More detailed studies combined with time-resolved optical and conductivity analysis are currently under way to scrutinize further this intriguing water oxidation cycle.

Acknowledgement

This work was supported by the Gas Research Institute, Chicago, IL, USA (subcontract with the Solar Energy Research Institute, Golden, CO) and the Nationaler Energie-Forschungs-Fonds (NEFF), Switzerland. M.K.N. thanks the Indian Government for financial assistance.

References

- 1 J. Biggins (ed.), *Progress in Photosynthesis Research*, Martinus Nijhoff, Dordrecht, 1987, Vol. 3.
- 2 (a) B. Kok, B. Forbush and M. McGloin, *Photochem. Photobiol.*, **14** (1971) 307; (b) P. Joliot, G. Barbieri and R. Chabau, *Photochem. Photobiol.*, **10** (1969) 309; (c) H. T. Witt, *Nouv. J. Chim.*, **11** (1987) 91; (d) O. Saygin and H. T. Witt, *Biochim. Biophys. Acta*, **893** (1987) 452.
- 3 G. C. Dismukes and Y. Siderer, *Proc. Nat. Acad. Sci. USA*, **78** (1981) 274.
- 4 G. W. Grudwig and R. H. Crabtree, *Proc. Nat. Acad. Sci. USA*, **83** (1986) 4586.
- 5 G. O. Lawrence and D. T. Saywer, *Coord. Chem. Rev.*, **27** (1978) 173.
- 6 J. B. Vincent and G. Christou, *FEBS Lett.*, **207** (1986) 250.
- 7 (a) J. E. Shants, R. S. Czernuszewicz, G. C. Dismukes, A. L. Rheingold, V. Petrouleas, J. A. Stubbe, W. H. Armstrong, R. H. Beer and S. J. Lippard, *J. Am. Chem. Soc.*, **109** (1987) 1345; (b) H. Diril, H. R. Chang, X. Zhang, S. K. Larsen, J. A. Potenza, C. G. Pierpont, H. J. Schugar, S. S. Isiod and D. N. Hendrickson, *J. Am. Chem. Soc.*, **109** (1987) 6207.
- 8 (a) H. Nijs, M. Cruz, J. J. Fripiat and H. Van Damme, *J. Chem. Soc., Chem. Commun.*, (1981) 1026; (b) H. Nijs, M. Cruz, J. J. Fripiat and H. Van Damme, *Nouv. J. Chim.*, **6** (1982) 551; (c) G. L. Elizarova, L. G. Matvienko, N. V. Nozhkina, V. E. Maizlish and V. N. Parmon, *React. Kinet. Catal. Lett.*, **16** (1981) 191; (d) V. N. Parmon, G. L. Elizarova and T. V. Kim, *ibid.*, **21** (1982) 195; (e) S. Goswami, A. R. Chakravarthy and A. Chakravarthy, *J. Chem. Soc., Chem. Commun.*, (1982) 1288; (f) V. Y. Shafrovich and V. V. Strelets, *Nouv. J. Chim.*, **6** (1983) 183; (g) B. S. Brunschwig, M. H. Chou, C. Creutz, P. K. Gosh and N. Sutin, *J. Am. Chem. Soc.*, **105** (1983) 4832; (h) G. Nord, B. Pederson and E. Bjergbakke, *ibid.*, **105** (1983) 1913; (i) H. Nijs, J. J. Fripiat and H. Van Damme, *J. Phys. Chem.*, **87** (1983) 1279; (j) P. K. Gosh, B. S. Brunschwig, M. H. Chan, C. Creutz and N. Sutin, *J. Am. Chem. Soc.*, **106** (1984) 4772; (k) R. B. Baar and F. C. Anson, *J. Electroanal. Chem.*, **187** (1985) 265; (l) M. M. Taqui Khan, R. C. Bhandwaj and C. M. Jadhar, *J. Chem. Soc., Chem. Commun.*, (1985) 1650; (m) R. Ramaruj, A. Kira and M. Kaneko, *Angew. Chem., Int. Ed. Engl.*, **25** (1986) 825; (n) K. Honda and A. J. Frank, *J. Chem. Soc., Chem. Commun.*, (1984) 1635; (o) J. P. Collins and J. P. Sauvage, *Inorg. Chem.*, **25** (1986) 135.
- 9 (a) S. W. Gersten, G. J. Samuels and T. J. Meyer, *J. Am. Chem. Soc.*, **104** (1982) 4029; (b) J. A. Gilbert, D. S. Eggleston, W. R. Murphy, D. A. Geselowitz, S. W. Gersten, D. J. Hodgson and T. J. Meyer, *ibid.*, **107** (1985) 3855.
- 10 F. P. Rotzinger, S. Munavalli, P. Comte, J. K. Hurst, M. Grätzel, F. J. Pern and A. J. Frank, *J. Am. Chem. Soc.*, **109** (1987) 6619.
- 11 F. P. Dwyer, H. A. Goodwin and E. C. Gyarfas, *Aust. J. Chem.*, **16** (1983) 42.
- 12 P. Liska, N. Vlachopoulos, M. K. Nazeeruddin, P. Comte and M. Grätzel, *J. Am. Chem. Soc.*, **110** (1988) 3686.
- 13 B. Durham, S. R. Wilson, D. J. Hodgson and T. J. Meyer, *J. Am. Chem. Soc.*, **102** (1980) 600.
- 14 B. A. Moyer and T. J. Meyer, *Inorg. Chem.*, **25** (1986) 2015.

- 15 D. A. Geselowitz, W. Kutner and T. J. Meyer, *Inorg. Chem.*, 25 (1986) 2015.
- 16 T. R. Weaver, T. J. Meyer, S. A. Adeyemi, G. M. Brown, R. P. Eckberg, W. E. Hatfield, E. C. Johnson, R. W. Murray and D. Unterecker, *J. Am. Chem. Soc.*, 97 (1975) 3039.
- 17 J. D. Dunitz and L. E. Orgel, *J. Chem. Soc.*, (1953) 2594.
- 18 M. Neumann-Spallart, K. Kalyanasundaram, C. K. Grätzel and M. Grätzel, *Helv. Chim. Acta*, 3 (1980) 1111.
- 19 F. Boletta, A. Juris, M. Maestri and D. Sandrini, *Inorg. Chim. Acta*, 44 (1980) L175.
- 20 P. S. Lay and W. H. F. Sasse, *Inorg. Chem.*, 24 (1985) 4707.
- 21 C. Creutz and N. Sutin, *Proc. Nat. Acad. Sci. USA*, 72 (1975) 2858.
- 22 V. Y. Shafirovich, N. K. Khannanov and V. V. Strelets, *Nouv. J. Chim.*, 4 (1980) 81.
- 23 U. Koelle, P. P. Infelta and M. Grätzel, *Inorg. Chem.*, 27 (1988) 879.
- 24 S. J. Raven and T. J. Meyer, *Inorg. Chem.*, 27 (1988) 4478.